Dettmering D., Schmidt M., Heinkelmann R., Seitz M. (2011): **Combination of different space-geodetic observations for regional ionosphere modeling.** Journal of Geodesy 85(12): 989-998

DOI:10.1007/s00190-010-0423-1

Combination of different space-geodetic observations for regional ionosphere modeling

Denise Dettmering · Michael Schmidt · Robert Heinkelmann · Manuela Seitz

Abstract Most of the space-geodetic observation techniques can be used for modeling the distribution of free electrons in the Earth's ionosphere. By combining different techniques one can take advantage of their different spatial and temporal distributions as well as their different observation characteristics and sensitivities concerning ionospheric parameter estimation.
The present publication introduces a procedure for multi-dimensional ionospheric modeling. The model consists of a given reference part and an unknown correction part expanded in terms of B-spline functions. This approach is used to compute regional models of Vertical Total Electron Content (VTEC) based on the International Reference Ionosphere (IRI 2007) and GPS observations from terrestrial Global Navigation Satellite System (GNSS) reference stations, radio occultation data from Low Earth Orbiters (LEOs), dual-frequency radar altimetry measurements, and data obtained by Very Long Baseline Interferometry (VLBI).
The approach overcomes deficiencies in the climatological IRI model and reaches the same level of accuracy than GNSS based VTEC maps from IGS. In areas without GNSS observations (e.g. over the oceans) radio occultations and altimetry provide valuable measurements and further improve the VTEC maps. Moreover, the approach supplies information on the offsets between different observation techniques as well as on their different sensitivity for ionosphere modeling. Altogether, the present procedure helps to derive improved ionospheric corrections (e.g. for one-frequency radar altimeters) and at the same time it improves our knowledge on the Earth's ionosphere.

Keywords Ionosphere · VTEC · Data Combination · B-splines

1 Introduction

Nowadays, most of the existing ionosphere models used in geodesy are based on terrestrial GNSS measurements. As the distribution of permanent GNSS reference stations is not globally uniform, the uncertainty of these models is also inconsistent all over the world. Regions covered by more reference stations can be described more precisely than others. In ocean areas where only some single stations are located on islands the data coverage is worst. However, these are the regions where dual-frequency satellite altimeters provide ionospheric data. In addition, GPS occultation measurements from Low Earth Orbiters can be used, which are available over continents as well as over oceans. A combination of the different measurement types will provide a higher and more consistent accuracy for VTEC maps than each measurement technique on its own as already shown by Todorova et al. (2007). Due to their diversity in frequencies and frequency separations each system shows a different sensitivity to ionospheric parameters. In the work presented here, four observation types (terrestrial GPS, space-based GPS, altimetry, and VLBI) are combined into one regional three-dimensional VTEC model. In a preprocessing step all observations are converted to VTEC up to one constant height. These values are then combined in one joint adjustment taking into account systematic offsets between the observation groups as well as their different accuracy levels.
The paper consists of five parts. Firstly, the general model approach is introduced followed by a description of the measurements used as input data (section 3) and the concept for data combination (section 4). Finally, the VTEC model results are presented (section 5) and validated against other models (section 6).

2 Multi-dimensional model approach

At the German Geodetic Research Institute (DGFI) a multi-dimensional model approach has been developed and published based on trigonometric and/or polynomial splines together with their tensor products, see e.g. Schmidt (2007) and Schmidt et al. (2008). As will be discussed in the following these base functions are compactly supported; thus, they have some advantages compared to spherical base functions, mainly for regional modeling but also for global models in case of unevenly distributed input observations and data gaps. Moreover, these base functions provide the possibility of a multi-resolution representation (Zeilhofer 2008).
The approach can be used for regional and global modeling of different ionospheric parameters. In this paper, the focus lies on the three-dimensional regional modeling of the VTEC depending on horizontal position φ, λ and on time t. The unknown $VTEC$ is separated into a reference part $VTEC_{\mathrm{ref}}$ taken from IRI 2007 (Bilitza and Reinisch 2008) and a correction part $\Delta VTEC$ which is modeled by a series expansion in tensor products of three systems of 1-D normalized endpoint-interpolating B-splines $\Phi_k^J(x)$ with $x \in \{\varphi, \lambda, t\}$ and unknown coefficients d_{k_1,k_2,k_3}. The basic observation equation reads

$$VTEC(\varphi,\lambda,t) = VTEC_{\mathrm{ref}}(\varphi,\lambda,t) + \Delta VTEC(\varphi,\lambda,t) \tag{1}$$

with

$$\Delta VTEC(\varphi,\lambda,t) = \sum_{k_1=0}^{K_1-1}\sum_{k_2=0}^{K_2-1}\sum_{k_3=0}^{K_3-1} d_{k_1,k_2,k_3}\Phi_{k_1}^{J_1}(\varphi)\Phi_{k_2}^{J_2}(\lambda)\Phi_{k_3}^{J_3}(t). \tag{2}$$

Each 1-D basis function system consists of $K = 2^J + 2$ single B-spline functions $\Phi_k^J(x)$ equally distributed on the unit interval as illustrated in Fig. 1 for J=4 (K=18). The number K of the functions depends on the level J of the spline. The corresponding recursive equation for the computation of $\Phi_k^J(x)$ is presented e.g. in Schmidt (2007). In the 1-D/2-D case the functions can be interpreted as peaks or caps whose number and sharpness increase with level J. As the observations will not be given in the unit-intervals in which the B-splines are defined a transformation from $[\varphi_{min},\varphi_{max}]\times[\lambda_{min},\lambda_{max}]\times[t_{min},t_{max}]$ to $[0,1]\times[0,1]\times[0,1]$ has to be done.

For the 3-D regional modeling in this paper levels J_1=4 for latitude, J_2=3 for longitude, and J_3=5 for the time are introduced, resulting in 18, 10 resp. 32 functions per dimension and 6120 unknown coefficients altogether. Therewith, for one day and an area of interest of $90°\times 90°$ a spatial resolution of about 5° resp. 9° and a temporal resolution of about 40 minutes can be reached.

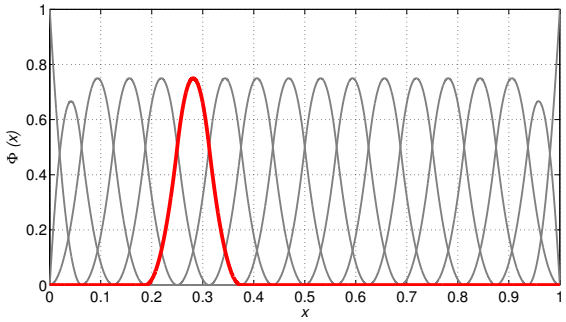

Fig. 1 The 18 1-D quadratic endpoint-interpolating B-spline functions of level $J = 4$. Each function is compactly supported, i.e. different from zero just in a finite interval which is illustrated by highlighting the 6th function in red color.

It is worth to be noticed that in contrast to many other approaches, a geographical coordinate system is used instead of a Sun-fixed one, e.g. (Dettmering 2003), or one based on modip latitude (Azpilicueta et al. 2006). This forces the parameterization of the time dependency but avoids the neglect of variations with local time.
The unknown coefficients d_{k_1,k_2,k_3} together with their formal errors are estimated within an adjustment process. Since each unknown coefficient is related to one 3-D compactly supported B-spline product $\Phi_{k_1}^{J_1}(\varphi)\Phi_{k_2}^{J_2}(\lambda)\Phi_{k_3}^{J_3}(t)$ centered at point $P(k_1,k_2,k_3)$ an unevenly distributed set of observations may cause an ill-conditioned or even singular normal equation system. To solve this problem the reference model is used as prior information, i.e. expectation values μ of the non-supported coefficients are introduced.
The unknown coefficients may be collected in one vector x and estimated within a Gauss-Markov model with functional part

$$Ax = l + e \tag{3}$$

and stochastic part

$$\Sigma(l) = \sigma_0^2 P^{-1} \tag{4}$$

where the observation vector l includes the $\Delta VTEC$ values, the design matrix A includes the inherent linear splines and the vector e represents the errors of the observations. The stochastic model is defined by the covariance matrix of the observations $\Sigma(l)$ composing of the weight matrix P and the unknown variance factor σ_0^2. In case of a matrix A with full column rank the

problem could be solved by

$$x = (A^T P A)^{-1} \cdot (A^T P l). \tag{5}$$

As different groups $i \in \{1...p\}$ of observations should be combined, p observation vectors l_i, design matrices A_i and weight matrices P_i exist. In addition, a reference model is introduced as prior information to overcome rank deficiencies of the normal equation system which occur if coefficients are not supported by measurements. Approximations for the unsupported coefficients are put in vector μ_x with weight matrix P_x. Moreover, different accuracy levels of the observation groups (with σ_i) and the prior information (with σ_x) are considered. Altogether this leads to the following extended normal equation system (Zeilhofer 2008):

$$\left(\sum_{i=1}^{p} \frac{1}{\sigma_i^2} A_i^T P_i A_i + \frac{1}{\sigma_x^2} P_x\right) x = \sum_{i=1}^{p} \frac{1}{\sigma_i^2} A_i^T P_i l_i + \frac{1}{\sigma_x^2} P_x \mu_x. \tag{6}$$

The different variance factors σ_i^2 and σ_x^2 are estimated within a VCE. In addition, for each observation group one constant offset is introduced in the model to allow for systematic differences between the data sets. More details on the combination strategy are given in section 4.

3 Input data

Measurements of four space-geodetic techniques (terrestrial GPS, space-based GPS, altimetry, and VLBI) are used. $VTEC$ observations are computed separately for each observation technique within a preprocessing procedure. All data sets are reduced by the corresponding reference values $VTEC_{\mathrm{ref}}$ to derive $\Delta VTEC$ values which serve as the input for the estimation of the unknown model coefficients. As reference model the International Reference Ionosphere IRI 2007 (Bilitza and Reinisch 2008) is used with standard input parameters. The distribution of all data used within this study is shown in Fig. 2. In addition to the reduced geodetic observations, zero-coefficients for the non-supported areas are introduced as prior information in order to overcome rank deficiencies of the normal equation system. In these areas the reference model will remain unchanged.

To assure a consistent combination of all data groups, only VTEC up to a height of 2000 km is accounted for, meaning that the plasmaspheric electron content has been reduced in the preprocessing and is not part of the model. For the reduction, resp. extrapolation from the different orbit heights to 2000 km a fraction approach based on IRI values is employed, developed by JPL to correct altimetry VTEC with GPS Global Ionospheric Maps (GIM), see Iijima et al. (1999) for more details. In case the model is employed to correct data from orbit heights other than 2000 km (e.g. GPS data) the same approach or an additional plasmaspheric model should be used.

In the following, the input data will be presented together with the most important preprocessing steps. All data used in this study are measured on May 3rd in 2007. All investigations are focused on a region of $90° \times 90°$ in the area of South America between $-60°$ and $+30°$ latitude and $-110°$ to $-20°$ longitude. To reduce the data amount and to ensure uncorrelated measurements (as no correlations between the observations will be introduced in the stochastic model) not all measurements are used within the parameter estimation but a data thinning is done for terrestrial GPS and altimetry data. The group definition is done per observation technique and mission/station (Jason-1, Envisat, COSMIC, CHAMP, two VLBI stations, and each GPS reference station). An overview on the used data is given in Table 1.

3.1 Terrestrial GPS

Terrestrial GPS data measured by the permanent reference stations of network SIRGAS-CON are used. More information on SIRGAS can be found in Sánchez and

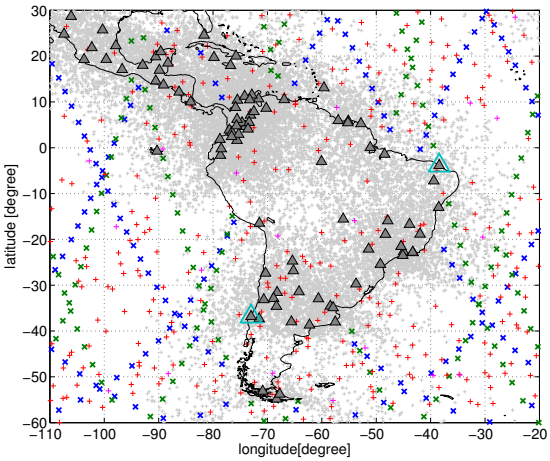

Fig. 2 Area under investigation and distribution of VTEC data for 24 hours on 2007-05-03. The blue/green crosses indicate the position of altimeter measurements from Jason-1/Envisat. Red and magenta crosses show the location of radio occultation profiles from COSMIC respectively CHAMP. GPS measurements together with reference stations are plotted in gray and the two VLBI stations marked in cyan.

Table 1 Summary of input data for 24 hours at 2007-05-03.

	Group No.	No. of data	Time spacing
Jason-1	1	128	30 sec
Envisat	2	118	30 sec
COSMIC	3	318	irregular
CHAMP	4	19	irregular
VLBI	5-6	47 (2 stations)	1 hour
GPS	7-104	19249 (98 stat.)	1 hour

Brunini (2009). For the day of investigation in May 2007 there are approximately 100 stations available which provide measurements to about 4 to 8 satellites with a sampling interval of 30 seconds.
For each receiver-satellite link code-leveled phase observations (Wilson and Mannucci 1994) are extracted and Slant Total Electron Content (STEC) is computed from the difference of the measurement at the two frequencies for all observations with zenith angle $z \leq 85°$ (elevation $\varepsilon \geq 5°$). The necessary formulae can be extracted e.g. from Dettmering (2003). In the next step STEC is converted to VTEC using the zenith angle z' from each observation at the ionospheric pierce point (intersection between signal path and shell height of ionospheric layer of the single-layer model). For this procedure, the modified single layer mapping function mf (MSLM) from Center for Orbit Determination in Bern (CODE) is used with $H = 506.7$ km, $\alpha = 0.9782$, and $R = 6371$ km (Hugentobler et al. 2002):

$$mf(z) = \frac{1}{\cos z'} \quad \text{with} \quad \sin z' = \tfrac{R}{R+H} \sin(\alpha \cdot z). \tag{7}$$

The GPS ionospheric observations always contain Differential Code Biases (DCB) in addition to the VTEC information due to different delays of the two signals within satellites as well as receivers. To account for these hardware offsets the DCBs have to be considered in the preprocessing. For satellite DCBs the values provided by IGS (Dow et al. 2009) are used. However, not for all SIRGAS stations receiver DCBs are available (only for IGS stations). Alternatively, own values are computed from a calibration with regard to IRI 2007. A comparison between these and IGS DCBs for the South American IGS stations shows an average agreement of 0.25 ns with variations of 1.6 ns (1σ) at the given day. For some stations the differences reach up to 4 ns (respectively 11 TECU). These large values result from an inaccurate IRI model but are not relevant for the VTEC modeling as long as a constant offset for each station is defined within the model (see section 4). Nevertheless, in future work it is intended to estimate own DCBs.

3.2 Altimetry

As only a few of the available satellite radar altimeters provide measurements at more than one frequency, the data source is limited to the following missions: TOPEX, Envisat (only till end of 2007) and Jason-1/2. For each of these missions 1 Hz data are available on fixed profiles with a repetition rate of 10 days for TOPEX and Jason, and 35 days for Envisat, leading to track separations at the equator of 315 km (TOPEX, Jason), respectively 80 km (Envisat). For May 2007 only data from Jason-1 and Envisat could be used, because these are the only active missions in this time interval.
Satellite radar altimeters directly measure the vertical distance between the orbit and the ocean surface. Thus, the ionospheric delay d_{ion} from measurements at two frequencies can easily be computed. VTEC below the satellite is proportional to this delay using equation (8). This approximation is valid for frequencies higher than 1 GHz (Langley 1998). No mapping function is necessary.

$$VTEC = STEC = -\frac{f^2}{40.3} \cdot d_{ion} \tag{8}$$

As the 1Hz observations are quite noisy a smoothing and thinning of the data is advantageous. For this purpose, a simple median filter with a length of 20 seconds (respectively about 120 km) has been applied as recommended by Picot et al. (2008). At last, an extrapolation of the data from orbit height to 2000 km is necessary in order to adapt them to the other data types. As for all other data types this is done following Iijima et al. (1999).

3.3 Space-based GPS

GPS Radio Occultation measurements on Low Earth Orbiters (LEOs) have two advantages compared with terrestrial GPS data. First, they are globally distributed and not limited to continental regions and second, they provide new measurement geometry probing the ionosphere on nearly horizontal links. In contrast to terrestrial GPS not only STEC data are provided but also vertical profiles of electron density and thereby the possibility to model the ionosphere in four dimensions (φ, λ, h, and t) (Hajj et al. 1994). However, in the following only the VTEC data computed from the vertical profiles are used.
Actually, there are several LEOs with occultation antennae available. For the following investigations data from the six satellites of the COSMIC/FORMOSAT-3 constellation (Fong et al. 2009) are used. This sys-

tem provides about 2000 globally distributed observations per day. In addition data from CHAMP satellite (Jakowski et al. 2002) are included. Integrated VTEC from the electron density profiles are available from UCAR/CDAAC.
Only the data from occultation antennae are used and the height extrapolation to 2000 km is done identical to the other techniques. Comparisons between COSMIC topside VTEC from POD antenna and IRI fractional approach used to do the height adaption show a general agreement better than 1 TECU (mean VTEC differences between LEO orbit height and GPS orbit height).

3.4 Very Long Baseline Interferometry (VLBI)

VLBI is a differential technique measuring around two center frequencies at X-band and S-band. In contrast to the other observation techniques single-difference group delays from signals arriving at two or more VLBI telescopes are measured. The ionospheric delay is given in the VLBI observation file provided by the IVS (Schlüter and Behrend 2007). It is proportional to the difference of the integral over the electron density along the signal path ($STEC'_{1,2}$) at the two observation sites 1,2 and includes a differential ionospheric offset:

$$d_{ion} = \frac{40.3}{f_x^2}[mf(\varepsilon_2)VTEC'_2 - mf(\varepsilon_1)VTEC'_1] + d_{\text{offset2}} - d_{\text{offset1}}. \quad (9)$$

The conversion from $STEC'$ to $VTEC'$ (the unknown VTEC at the ionospheric pierce points) is done based on a mapping function mf given by IERS (2010) and depending on the elevation angle ε of the observation:

$$mf(\varepsilon) = \frac{1}{\sqrt{1 - \frac{r^2 cos^2 \varepsilon}{(r+h)^2}}}. \quad (10)$$

The variable r is the geocentric distance of the specific site and $h = 450$ km the adopted effective height of the thin shell approximation of the ionosphere lying close to the height of the F_2 peak of the electron density (Hobiger et al. 2006). Some easy rearrangements will lead to the same form as equation (7) with different shell heights (H/h), different constant α (0.9782/1.0) and different stations heights (R/r). Maximum differences of about 0.2 occur for zenith distances of 85° (r=R=6371 km). These are up to 8% difference for GPS and VLBI mapping. Using the CODE mapping function (7) for the VLBI preprocessing will lead to nearly constant offsets in the VLBI VTEC (about 1 to 2 TECU, depending on the observations site). These differences are assimilated by the estimated inter-technique biases and are part of the values which are shown in Table 2. For further investigations identical mapping functions will be used.
The observation equation (9) relates four unknown parameters to each observation. It is evident that a redundant estimation of the parameters can only be achieved by gathering some observations together, which depend on the same parameters. Therefore, $VTEC'$ at the specific ionospheric pierce point is modeled as a function of $VTEC$ above the telescope, depending on the position of the telescope φ, λ and the ionospheric pierce points φ', λ', as well as on two gradients G_n, G_s in north and south direction:

$$VTEC'(t) = \left(1 + (\varphi' - \varphi) \begin{bmatrix} G_s \\ G_n \end{bmatrix}\right) VTEC(t + (\lambda' - \lambda)/15). \quad (11)$$

The longitudinal difference is temporally related to the observation site assuming that the ionosphere remains constant during the (short) duration Earth takes to rotate the angle of longitudinal difference, i.e. the epoch of the ionospheric delay observation is shifted forward or backward in time until the longitudes of the specific pierce point and the observation site would coincide. The latitudinal difference is modeled by two gradients which are solved in the estimation process together with $VTEC$. The singularity caused by the unknown ionospheric offsets is compensated by setting the sum over the offsets to zero (Sekido et al. 2003).
For the area and time under investigation two VLBI telescopes can provide data: Fortaleza in Brazil and Tigo/Concepción in Chile. For both stations VTEC values with a time resolution of 1 hour are introduced into the model.
Naturally, VLBI will provide much less data than other techniques as only one measurement per baseline can be taken at a given epoch. In contrast, one GPS receiver observes between four and ten (in case of GNSS even more) satellites. In addition, only few VLBI observation sites exist – coinciding with GPS permanent stations in most cases. Nevertheless, it seems useful to include VLBI measurements in the VTEC combination to increase the redundancy and the reliability of the model. Existing offsets to other observation techniques (see e.g. Bergstrand and Haas (2004)) are estimated within the adjustment and different accuracy levels are considered by the VCE.

4 Combination strategy

As already stated, in this study data from different space-geodetic techniques but of the same observation

type (VTEC) are combined, which are derived from the original observations within the preprocessing. As a consequence, direct measurements of the target parameter are available. In the functional model there is no difference to an adjustment using only one measurement technique. However, the stochastic model (Eq. 4) has to be extended because the accuracy level of the observations is not necessarily identical for all groups. Instead of one common a-posteriori variance factor σ_0^2, an individual variance factor σ_i^2 for each observation group $i \in \{1...p\}$ is introduced to enable different weighting for each group. No correlations are introduced and the weight matrices P_i are assumed to be known. The extended stochastic model is given by

$$\Sigma(l) = \begin{pmatrix} {\sigma_1}^2 {P_1}^{-1} & 0 & \cdots & 0 \\ 0 & {\sigma_2}^2 {P_2}^{-1} & & 0 \\ \vdots & & \ddots & \vdots \\ 0 & 0 & & {\sigma_p}^2 {P_p}^{-1} \end{pmatrix}. \qquad (12)$$

As no realistic variance-covariance matrices for all data types are available no weighting within the observation groups is done and no correlations are introduced. Instead unit matrices are used as weight matrices:

$$P_i = I. \qquad (13)$$

In an iterative approach, each σ_i^2 can be computed from the observation group residuals. For solving this problem in an efficient way a fast Monte-Carlo implementation of the iterative maximum-likelihood Variance Component Estimation (MCVCE) is applied as given by Koch and Kusche (2002).

Within the combination process not only the measurements have to be handled but also the prior information. The latter are introduced as pseudo observations in areas where no direct measurements exist. This is necessary to overcome rank deficiencies from unevenly distributed observations (see section 2). The prior information is included in the VCE and an additional variance component σ_x^2 is estimated for the reference model.

By means of the VCE the different stochastic characteristics of the observation techniques are taken into account. Table 2 shows the variance components for all six observation groups. It can be seen that the Envisat observations gets the maximum weight, followed by Jason-1, COSMIC, CHAMP, and the two VLBI stations. The reference model's variance component is estimated to be $\sigma_x = 5.06$.

In addition, systematic differences in the functional model might occur, i.e. offsets between the absolute VTEC measurements. This is already known from prior investigations, e.g. by Brunini et al. (2005). These offsets or biases may be caused by insufficient calibration (Azpilicueta and Brunini 2009) and/or errors introduced by inaccurate model assumptions (e.g. mapping function for terrestrial GPS measurements).

Table 2 Estimated relative biases (technique minus mean GPS) and their precision, together with estimated variance components from VCE

	Bias w.r.t. mean GPS [TECU]	Variance Components σ_i [-]
Jason-1	$+2.4 \pm 0.2$	1.45
Envisat	-2.2 ± 0.2	0.96
COSMIC	-2.1 ± 0.1	1.58
CHAMP	-1.9 ± 0.9	3.77
VLBI Fort.	-0.4 ± 1.8	3.84
VLBI Tigo	-2.1 ± 0.8	3.66

In the presented model approach, up to one time-constant bias term per observation group is allowed. It is likely that the offsets are not constant over a longer time period. However, as only time spans up to one day per model will be processed (leading to daily constants for the bias terms), the time variability can be neglected. The obtained biases are relative values with respect to the reference model used for the computations, i.e. with respect to IRI 2007. The usage of other reference models will result in significant other bias values. As a consequence, only the relative biases between the observation techniques which are shown in Table 2 should be interpreted. All GPS measurements are already reduced by the DCBs within the preprocessing and the estimated biases are – except for remaining effects due to wrong DCBs – free of them (same for site-specific VLBI offsets). Impacts due to different orbit heights are minimized by the height reduction.

For further details on the inter-technique biases as well as on the results of VCE see Dettmering et al. (submitted) where – among other things – special emphasis is given to time variable effects.

5 VTEC maps

The main result of the parameter estimation are the B-spline coefficients d_{k_1,k_2,k_3} which may be used to compute VTEC values for every location within the region under investigation and during the modeled time interval. However these coefficients are not easy to interpret. They reach values between approximately ± 20 TECU. Out of 6120 coefficients, 258 are zero and about the same number are close to zero (thus not significant) due to no or sparse measurements and/or good agreement to the reference model which remains unchanged in these regions.

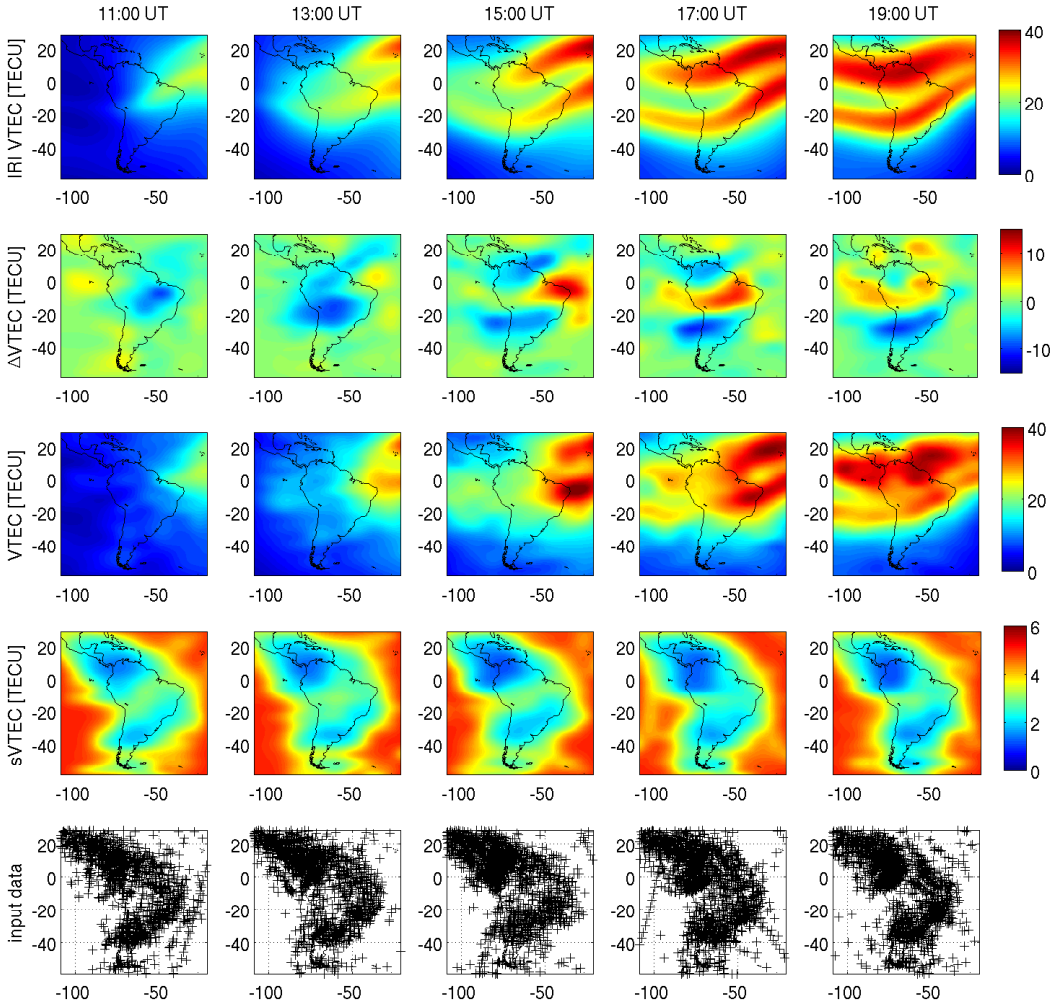

Fig. 3 Estimated VTEC for 5 epochs on 2007-05-03. The first row shows the reference $VTEC_{\mathrm{ref}}$, second row the estimated $\Delta VTEC$, third row the new $VTEC$, and forth row the standard deviations of estimated VTEC, all in TECU. In the last row the input data distribution is plotted.

The model coefficients may be used in a reconstruction process to determine $\Delta VTEC$ for specific locations and times and to combine it with the reference model $VTEC_{\mathrm{ref}}$ to $VTEC$ according to Eq.(1). In the following, regular VTEC grids of $1^\circ \times 1^\circ$ at each integer hour of the day are computed together with error estimates for each VTEC value. It is important to note, that – even if the VTEC is derived only for discrete epochs – it is available on a continuous basis as the time is also parameterized by splines. Fig. 3 displays a subset of these grids. Each column of the figure represents one epoch in Universal Time (UT) with a separation of 2 hours between each other. The first row illustrates $VTEC_{\mathrm{ref}}$ (IRI 2007), the second one the estimated $\Delta VTEC$, the third and the fourth row show the resultant VTEC maps together with their precision. In addition, the observations introduced in the models are plotted in the last row. The estimated differences to the reference model IRI 2007 vary by about ± 15 TECU. The figure clearly demonstrates that these differences could only be computed in areas where enough data are available: in regions without observations the $\Delta VTEC$ is always zero. The influence area of single measurements is defined by the model resolution and thus by the level of the B-spline modeling. The observation distribution is also reflected by the uncertainties of VTEC: in regions with many data points, precision of about 1 TECU is reached whereas the precision is only around

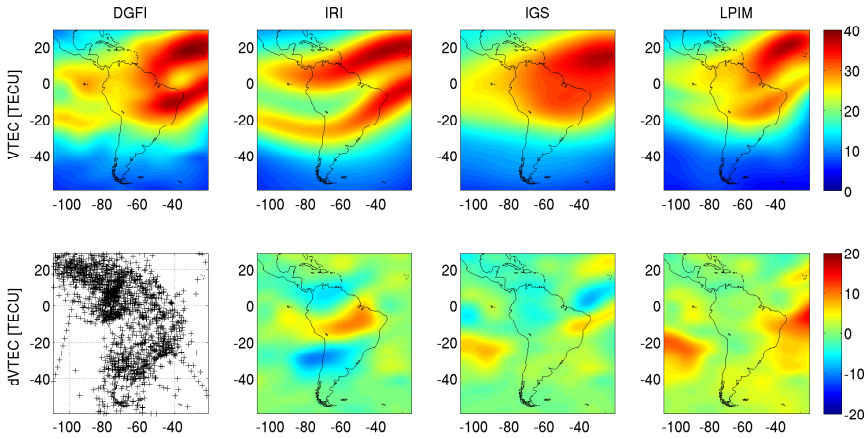

Fig. 4 VTEC maps from different models for 2007-05-03, 17 UT together with their differences to estimated VTEC by the approach under investigation (DGFI). In the first row the absolute VTEC values are plotted and in the second row their differences w.r.t. DGFI approach. The first plot in the second row is showing the data distribution used for estimating the DGFI model.

5 TECU over the oceans and at epochs without data contribution where the main error component is due to reference model uncertainties.

6 Comparison with other VTEC maps

VTEC maps are available from many institutions. Most of them are based on terrestrial GNSS measurements. The most important are the GIMs of IGS which combine results of five different analysis centers (Hernández-Pajares et al. 2009) working with diverse modeling approaches but basically with the same data set of IGS stations. GESA (Georreferenciación Satelitaria, at University of La Plata, Argentina) provides another possibility for comparison: regional ionosphere maps of South America are produced using the La Plata Ionospheric Model (LPIM), see Brunini at al. (2008). This model is independent from IGS processing (using e.g. modip latitude) but is based in parts also on IGS data. These two GNSS GIMs are used to validate the estimated VTEC maps on May, 3rd in 2007. In Fig. 4 the results are plotted exemplarily for 17:00 UT.

At 17:00 UT on this specific day the differences of the estimated VTEC in the area under investigation reach rms (mean/max) values of 3.1 (-0.3/10.5) TECU with respect to IRI 2007, 2.6 (-0.2/8.4) TECU w.r.t. IGS, and 2.9 (2.6/16.1) TECU w.r.t. LPIM. While the main differences to IRI occur in the continental areas, the major changes with respect to the GNSS based models of IGS and LPIM can be seen over the oceans. That means that the second plot in the second row mainly shows the improvements to IRI generated by the introduction of geodetic observations whereas in the last two plots of the second row the signal is basically due to model differences between IRI and GPS GIM which cannot be reduced in some parts of the oceanic areas because of missing input data. All differences are smaller than the formal error of VTEC taking a confidence level of 99% (3σ) into account leading to maximal errors of about 15 TECU for most of the ocean areas (see Fig. 3, fourth row, fourth panel).

As all these comparisons only reveal relative differences of the various models no information is given on the absolute quality and it is not obvious which of these models is better than the others and which one is the best. If taken into account that no actual measurements are assimilated into IRI the assumption that this model is not as reliable as the GPS based ones may be justified. The question if LPIM or IGS is more accurate is much more difficult. For the further comparisons IGS is chosen as reference because it is computed from 5 (more or less) independent models and thus should be more reliable, even if the regional LPIM with its better data coverage may be more accurate. Unfortunately, LPIM does not provide any error information. The accuracies given within the IGS model are – with values smaller than 2 TECU for most parts of the model – quite optimistic and not reliable. Only in some regions and at some epochs larger values up to about 4 TECU occur. The differences between the models from the different processing centers are larger than this (up to 12 TECU between CODE and JPL solution on 2007-05-03).

If IGS is taken as reference the DGFI model approach can improve the IRI 2007 by about 1 TECU rms from 3.0 to 1.9 TECU as illustrated by the histograms in Fig. 5. In addition, the differences between DGFI and IGS are almost normally distributed while they show a clear systematic between IRI and IGS. Both histograms

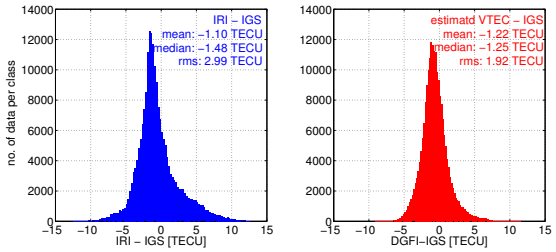

Fig. 5 Histogram showing the differences to IGS VTEC model for IRI 2007 (reference model) on the left side and for estimated VTEC on the right. Computed from 24 hour and the whole area under investigation for a regular grid of $\Delta t = 1h$ and $\Delta\varphi = \Delta\lambda = 1°$.

contain a small offset (class with most differences) of about -1.6 TECU (IRI) resp. -1.1 TECU (DGFI). The differences to LPIM are larger for IRI as well as for DGFI model. However, the mean value as well as the rms of the differences can be reduced by the DGFI approach from 2.8/3.4 TECU to 2.6/2.4 TECU.

It is important to keep in mind, that the improvements are only locally in regions and during times where input data are actually available. Consequently, a good reference model as well as a well-balanced matching between observation distribution and model resolution is necessary to compute high quality VTEC models.

7 Conclusion and outlook

As shown in the previous sections a combination of different observation techniques for ionospheric modeling is possible and reasonable. Reliable VTEC maps with high resolution and accuracies better than 2 TECU can be achieved when considering the systematic offsets as well as the accuracy levels of the different data sets. The presented B-spline approach allows regional or local improvements of existing VTEC maps which are used as reference model. However, improvements are only possible in areas and during times with data input; in other regions the reference model will remain unaffected but also no unintended effects occur, such as ringing in special harmonic expansions. In case of bad data coverage the use of an accurate and reliable reference models is recommended to avoid strong regional accuracy differences.

The example processed here shows that the approach can overcome deficiencies of the climatological model IRI and reach the same level of accuracy as models from IGS and LPIM. In areas with good data coverage it is probably better than these since better model resolutions are possible. Especially, this is the case in oceanic regions where only sparse terrestrial GPS data are available. These gaps are filled by altimeter measurements and radio occultation data. In continental areas with dense GPS observations the improvement by the other measurement techniques will be much smaller.

The result presented here is only a snapshot for one specific day and a longer time period for evaluation would be preferable. Nevertheless, the period under investigation represents quiet solar and geomagnetic conditions. Even more improvements are expected for other solar cycle periods by the integration of geodetic measurements in the climatological IRI model.

The VTEC modeling benefits from the improved data coverage of a combination of different space-geodetic observations. However, the different measurement geometry of the techniques is not totally capitalized as all observations were reduced to VTEC. A full exploitation of the different measurement characteristics may be achieved by combining all data into one four-dimensional model of electron density. The different intersecting angles of the signals will lead to a reliable estimation of the vertical electron density distributions in addition to the temporal and horizontal ones.

To improve the data combination and to reach more realistic error estimates the use of full and realistic noise variance-covariance matrices for all observation groups will be essential. Moreover, in order to further improve the reliability of the models and to homogenize their precision (in time and space) a dense and uniform data distribution is necessary. For this purpose more data types could be integrated in the model, e.g. radio occultation measurements of GRACE, TerraSAR-X and other LEO missions as well as VTEC data from additional altimeter missions and DORIS two-frequency measurements, preferably together with realistic information on their accuracies.

Acknowledgements This work is based on the observations of space-geodetic measurement techniques and models kindly provided by AVISO, ESA, GESA, IGS, IVS, NASA, and UCAR.

References

Azpilicueta, F., and C. Brunini. Analysis of the bias between TOPEX and GPS vTEC determinations. Journal of Geodesy 83(2), 121-127 (2009)

Azpilicueta, F., C. Brunini, and S.M. Radicella. Global ionospheric maps from GPS observations using modip latitude. Advances in Space Research 38, 2324-2331 (2006)

Bergstrand, S., and R. Haas. Comparison of Ionospheric Activity Derived from GPS and Different VLBI Networks. IVS General Meeting Proceedings, 447-451 (2004)

Bilitza, D., and B.W. Reinisch. International Reference Ionosphere 2007: Improvements and new parameters. Advances in Space Research, 42(4),599-609 (2008)

Brunini, C., A. Meza, and W. Bosch. Temporal and spatial variability of the bias between TOPEX- and GPS-derived total electron content. Journal of Geodesy, 79(4-5), 175-188 (2005)

Brunini, C., A. Meza, M. Gende, and F. Azpilicueta. South American regional ionospheric maps computed by GESA: A pilot service in the framework of SIRGAS. Advances in Space Research, Vol. 42(4), 737-744 (2008)

Dettmering, D. Die Nutzung des GPS zur dreidimensionalen Ionosphärenmodellierung. Department of Geodesy and Geoinformatic, Stuttgart, University of Stuttgart (2003)

Dettmering, D., Heinkelmann, R., and Schmidt, M. Systematic differences between VTEC obtained by different space-geodetic techniques during CONT08. Journal of Geodesy (submitted)

Dow, J.M., R. E. Neilan, and C. Rizos. The International GNSS Service in a changing landscape of Global Navigation Satellite Systems. Journal of Geodesy, 83, 191-198 (2009)

Fong, C.-J., N. L. Yen, C.-H. Chu, S.-K. Yang, W.-T. Shiau, C.-Y. Huang, S. Chi, S.-S. Chen, Y.-A. Liou, and Y.-H. Kuo. FORMOSAT-3/COSMIC Spacecraft Constellation System, Mission Results, and Prospect for Follow-On Mission. Terrestrial, Atmospheric and Oceanic Science, 20, 1-19 (2009)

Hajj, G.A., R. Ibañez-Meier, E.R. Kursinski, and L.J. Romans. Imaging the ionosphere with the Global Positioning System. International Journal of Imaging Systems and Technology, 5, 174-184 (1994)

Hernández-Pajares, M., J. M. Juan, J. Sanz, R. Orus, A. Garcia-Rigo, J. Feltens, A. Komjathy, S. C. Schaer, and A. Krankowski. The IGS VTEC map: a reliable source of ionospheric information since 1998. Journal of Geodesy, 83(3-4), 263-275 (2009)

Hobiger, T., T. Kondo, and H. Schuh. Very long baseline interferometry as a tool to probe the ionosphere. Radio Science, 41(1),RS1006 (2006)

Hugentobler, U., S. Schaer, G. Beutler, H. Bock, R. Dach, A. Jäggi, M. Meindl, C. Urschl, L. Mervart, M. Rothacher, U. Wild, A. Wiget, E. Brockmann, D. Ineichen, G. Weber, H. Habrich, and C. Boucher. CODE IGS Analysis Center Technical Report 2002 (2002)

IERS. IERS Conventions update, web resource. http://tai.bipm.org/iers/convupdt/convupdt_c9.html (2010)

Iijima, B. A., I. L. Harris, C. M. Ho, U. J. Lindqwister, A. J. Mannucci, X. Pi, M. J. Reyes, L. C. Sparks, and B. D. Wilson. Automated daily process for global ionospheric total electron content maps and satellite ocean ionospheric calibration based on Global Positioning System. Journal of Atmospheric and Solar-Terrestrial Physics, 61(16), 1205-1218 (1999)

Jakowski, N., A. Wehrenpfennig, S. Heise, Ch. Reigber, H. Lühr, L. Grunwaldt, and T.K. Meehan. GPS radio occultation measurements of the ionosphere from CHAMP: Early results. Geophysical Research Letters, Vol. 29(10), 10.1029/2001 (2002)

Koch, K.R., and J. Kusche. Regularization of geopotential determination from satellite data by variance components. Journal of Geodesy, 76(5),259-268 (2002)

Langley, R. B. Propagation of the GPS Signals. Chap. 3 in GPS for Geodesy, by P. J.G. Teunissen and A. Kleusberg [Eds.], Springer, Berlin, Heidelberg (1998)

Picot, N., K. Case, S. Desai, and P. Vincent. AVISO and PO-DAAC User Handbook. IGDR and GDR Jason Products, Edition 4.1. Report SMM-MU-M5_OP-13184-CN (AVISO), JPL D-21352 (PODAAC) (2008)

Sánchez, L., and C. Brunini. Achievements and Challenges of SIRGAS. IAG Symposia, Vol. 134. Springer, 161-166 (2009)

Schlüter, W., and D. Behrend. The International VLBI Service for Geodesy and Astrometry (IVS): current capabilities and future prospects. Journal of Geodesy, 81(6-8), 379-387 (2007)

Schmidt, M. Wavelet modelling in support of IRI. Advances in Space Research, 39(5) , 932-940 (2007)

Schmidt, M., M.O. Karslioglu, and C. Zeilhofer. Regional multi-dimensional modeling of the ionosphere from satellite data. Proceedings of the TUJK Annual Scientific Meeting. Ankara (2008)

Sekido, M., T. Kondo, E. Kawai, and M. Imae. Evaluation of GPS-based ionospheric TEC map by comparing with VLBI data. Radio Science, 38(4), doi:10.1029/2000RS002620 (2003)

Todorova, S., H. Schuh, T. Hobiger, and M. Hernández-Parajes. Global models of the ionosphere obtained by integration of GNSS and satellite altimetry data. Österreichische Zeitschrift für Vermessung und Geoinformation (VGI), 2, 80-89 (2007)

Wilson, B. D., and A. J. Mannucci. Extracting Ionospheric Measurements from GPS in the Presence of ANTI-Spoofing. Proceedings of the ION GPS-94. Salt Lake City (1994)

Zeilhofer, C. Multi-dimensional B-spline Modeling of Spatio-temporal Ionospheric Signals. DGK Reihe A123, Deutsche Geodätische Kommission, München (2008)